Journal of Engineering Mathematics **44:** 173–198, 2002.

Microwave heating of laminate panels

G. A. KRIEGSMANN and B. S. TILLEY[1]
Department of Mathematical Sciences, Center for Applied Mathematics and Statistics, New Jersey Institute of Technology, University Heights Newark, NJ 07102, U.S.A.
[1]*Franklin W. Olin College of Engineering, 1735 Great Plain Avenue Needham, MA 02492, U.S.A.*

Received 21 November 2001; accepted in revised form 3 June 2002

Abstract. The use of microwaves to heat laminate panels occurs in a variety of industrial processes, from chemical vapor infiltration (CVI) systems to the curing of adhesives in laminate panels. The electrical conductivity of the materials used in these systems is typically temperature-dependent. Characteristically, the thickness of the laminate panel is on the order of wavelength of the incident microwave, but the thickness of the laminate sheet is much smaller. This allows us to apply asymptotic techniques to find averaged wave and heat equations when the direction of the incident microwave is normal to, or tangent to, the laminates. These equations are analyzed in the small-Biot-number limit and are numerically approximated using finite differences. The results are in excellent agreement for small Biot numbers. More importantly, heating trends are observed for a wide variety of volume fractions for two particular CVI applications. In addition, the effect of the incident polarization on the heating process are also established. In particular, the use of a TE polarized incident microwave is shown to be inefficient in certain CVI applications, but produces a more favorable temperature gradient.

Key words: asymptotics, chemical vapor infiltration, laminate panels, microwave heating, small Biot-number

1. Introduction

The physical problems modeled and analyzed in this paper are motivated by the wish to understand certain aspects of microwave-assisted chemical vapor infiltration. In this process microwaves are used to heat a fibrous ceramic preform in the presence of a reacting gas. This gas reacts with the fibers composing the preform and fills in the interstitial spaces with material. If this filling process is complete and uniform, then a ceramic composite is fabricated with a built-in fiber skeleton. This technique, although beset by many challenging problems, has the potential to produce high-quality ceramic composites of arbitrary shape [1, 2].

One particular technique to construct composite panels is to alternately layer two types of thin fibrous sheets and then apply microwaves in the presence of a reacting gas. This is done, for example, to produce composite silicon-carbide (SiC) panels for high-temperature applications [2]. In this process the first sheet is made of SiC fibers. The second is the same sheet, except it has been embedded with carbon particles to enhance the electrical conductivity.

In this paper we model and study the microwave heating portion of this process as a prelude for a more complete study involving the reacting gas. Specifically, we model each SiC sheet as a thin ceramic slab which is characterized by its electrical and thermal parameters. Our objective is to understand how microwaves heat the laminate composite constructed from these thin slabs. In particular, we are concerned with the important issues of nonuniform heating and thermal runaway. The former can be useful; if the interior is at a higher temperature, then the gas will react with this region first and the preform will be filled from the inside to the exterior, which is a desirable feature [4–10]. The latter can be disastrous; a slight change in

input power can cause the temperature to jump beyond the melting point of the material. The geometry we consider is shown in Figure 1a where the first slab has a thickness αD, and the second, $(1-\alpha)D$, where the thickness $D \ll \lambda$, the wavelength of the incident microwave. The total thickness off the panel $L \sim \lambda$, so that many layers are required to construct this composite.

Although the above model takes into account the microstructure of the thin constitutive ceramic slabs which make up the laminate composite, it does neglect their individual porosities. The description of the electromagnetic heating of a laminate composite which takes into account a rigorous description at the pore scale is indeed difficult.

An idealized model of microwave-assisted chemical vapor infiltration considered the presence of a single pore whose effect on the electromagnetic fields was ignored [6]. This decoupled the electromagnetic portion of the problem from the heat transfer and chemical parts, both described by one-dimensional equations, and allowed a simplified analysis which described pore filling and closure. Although this model gives a considerable amount of insight into this complicated process, the inclusion of a more complicated porous structure necessitates a more careful description of the microwave interaction and heating of the material.

Motivated by the above study we shall model the microwave heating of the laminate structure shown in Figure 1b. Here the alternating slab constituents are the material and the gas-filled pore; the former has thickness αD, the latter $(1-\alpha)D$. Again, the thickness $D \ll \lambda$. Our model is two-dimensional, which allows a simple scalar description of the electromagnetic fields, and takes into account electromagnetic and thermal coupling. This two-dimensional assumption is a physical compromise between the single-pore model and the realistic three-dimensional model. The latter is much more difficult to analyze, requiring variational techniques to unwind the modal character of the electromagnetic propagation in the structure [10].

The remainder of the paper will now be outlined. In Section 2 we present a general formulation which describes the microwave heating of both laminate structures. In Section 3 we present two asymptotic analyses which produce averaged equations that describe the heating processes. In the first we apply the method of multiple scales and obtain standard homogenization results for the one-dimensional heat and reduced wave equations; it is presented here for completeness. In the second we apply a regular perturbation expansion to the two-dimensional heat and reduced wave equations. The result is an averaged heat equation with averaged boundary conditions. However, the form of the averaged reduced wave equation and the source term in the heat equation depend critically upon the polarization of the incident wave. We note here that, although the motivation for deriving these averaged equations comes from microwave-assisted chemical vapor infiltration, these equations hold for other heating scenarios involving laminated structures.

In Section 4 we obtain approximate solutions to our equations in the small-Biot-number limit. Here the temperature to leading order is spatially independent, but depends on time and the electric field through a spatially averaged source term. These results are similar to those for a solid slab [11,12], but differ significantly in the pore problem when the electric field of the incident microwave is aligned with the Y-axis.

Section 5 contains our numerical results for the steady state temperatures of both laminate panels and our small Biot number approximations. These produce S-shaped response curves that are similar to those obtained for solid slabs [11]. The dependence of these curves on laminate thickness, polarization, and other physical properties is discussed and contrasted.

Finally, in Section 6 we offer a short conclusion.

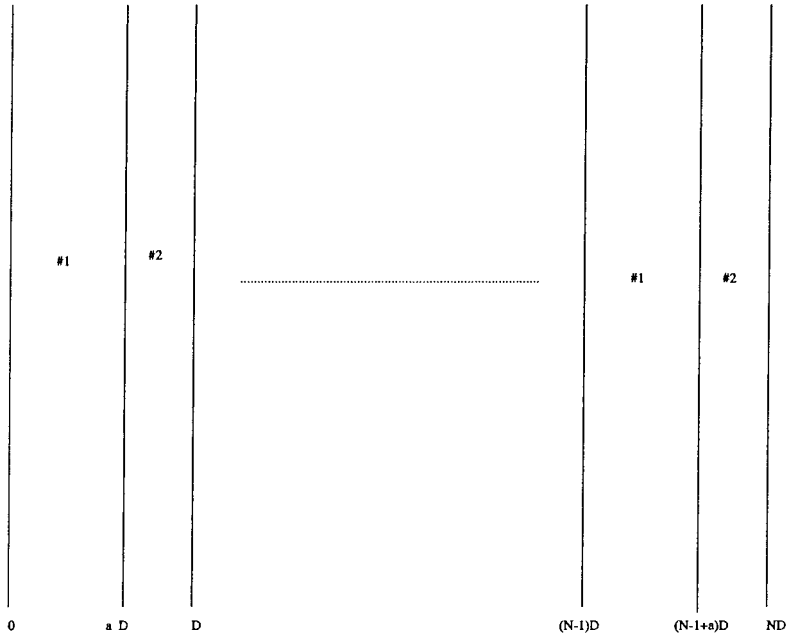

FIGURE 1A

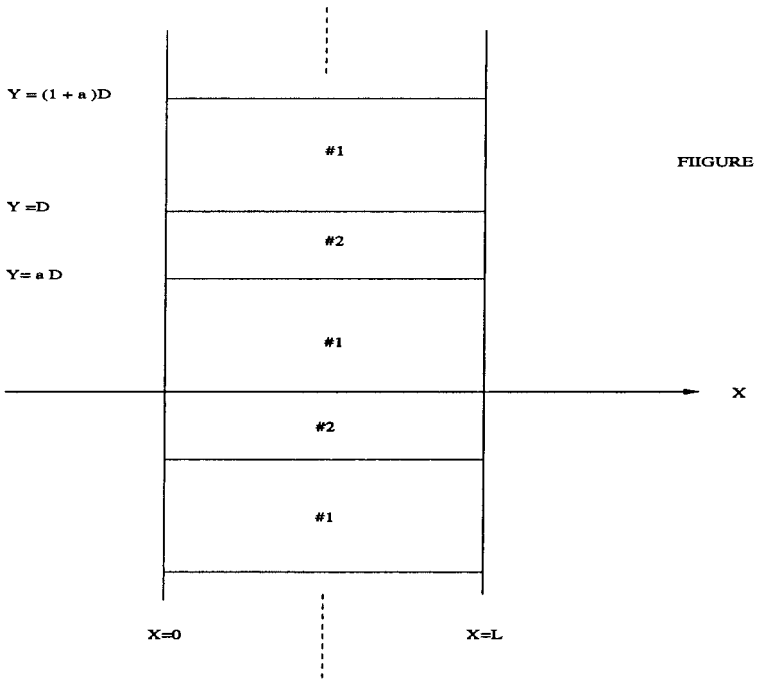

FIIGURE 1B

Figure 1. Two problems under consideration: propagation vector perpendicular to the laminate direction (*P*); propagation vector tangential to the laminate direction (*T*).

2. Formulation

We wish to study the microwave heating of two types of laminate panels composed of two alternating slabs made of different materials. These materials are characterized by different thermal and electrical properties. In both cases the panels occupy the region $0 < X < L$. The first laminate panel is sketched in Figure 1a and its slab boundaries are planes perpendicular to the X-axis. The second is sketched in Figure 1b and its slab boundaries are parallel to the X-axis. In both cases the panels are heated by a plane electromagnetic wave, incident from $X = -\infty$ and propagating in the $+X$-direction. Accordingly, we shall call the first case the $\mathcal{P}$ problem, because the incident wave vector $\mathbf{k}' = \omega/C_0\hat{\mathbf{x}}$ is perpendicular to the slab interfaces, and the second the $\mathcal{T}$ problem, because $\mathbf{k}$ is tangent to these interfaces. Here ω is the angular frequency of the incident wave and C_0 is the speed of light in free space; a time dependence of $\mathrm{e}^{-\mathrm{i}\omega t'}$ is assumed throughout, and suppressed.

In the $\mathcal{P}$ problem the incident electric field is taken to be $\mathbf{E}_{inc} = E_0\mathrm{e}^{\mathrm{i}k'X}\hat{\mathbf{z}}$, where E_0 is its strength. This is done without loss of generality because the geometry of the laminate structure is rotationally invariant in the YZ-plane. Consequently, the total electric field $\mathbf{E}$ is given in the free-space regions $X < 0$ and $X > L$ by

$$\mathbf{E} = E_0[\exp(\mathrm{i}k'X) + \Gamma\ \exp(-\mathrm{i}k'X)]\hat{\mathbf{z}} \quad X < 0, \tag{1a}$$

$$\mathbf{E} = E_0[\Upsilon\ \exp(\mathrm{i}k'X)]\hat{\mathbf{z}}, \quad X > L, \tag{1b}$$

respectively, where Υ is the transmission coefficient, and Γ is the reflection coefficient. Both Υ and Γ are to be determined.

The electric field which penetrates the laminate panel and interacts with the material slabs is given by $\mathbf{E} = E_0U(X)\mathbf{z}$, where the dimensionless function U satisfies

$$\frac{\mathrm{d}^2U}{\mathrm{d}X^2} + k'^2[N^2(X/D) + \mathrm{i}\frac{\sigma_0}{\omega\epsilon_0}f(-1 + T/T_0,\ X/D)]U = 0, \qquad 0 < X < L. \tag{2a}$$

In this equation ϵ_0 is the permittivity of free space, $N^2(X/D)$ is the index of refraction, T_0 is the ambient temperature in the absence of microwave radiation, T is the temperature of the slab in the presence of radiation, σ_0 is the conductivity of the slab at T_0, and $f(-1 + T/T_0,\ X/D)$ is the conductivity of the slab normalized by σ_0, *i.e.*, $f(0) = 1$. We take $T_0 =$ 300 K and σ_0 to be the electrical conductivity of SiC at this temperature. Both N^2 and f are piecewise constant on each material slab. Implicit in (2a) is our assumption that the magnetic permeability of the constituent slabs is identical to that of free space, μ_0.

From the continuity of the tangential electric and magnetic fields at $X = 0$ and $X = L$, we deduce that U and its derivative are continuous there. Combining this fact with (1) and eliminating Υ and Γ, we find that U satisfies the boundary conditions

$$\frac{\mathrm{d}U}{\mathrm{d}X} + \mathrm{i}k'U = 2\mathrm{i}k', \qquad X = 0, \tag{2b}$$

$$\frac{\mathrm{d}U}{\mathrm{d}X} - \mathrm{i}k'U = 0, \qquad X = L. \tag{2c}$$

Since both the electric field and the laminate properties only depend upon X, the temperature T satisfies the one-dimensional heat equation

$$\rho C_p \frac{\partial}{\partial t'} T = \frac{\partial}{\partial X}\{K \frac{\partial}{\partial X} T\} + E_0^2 \frac{\sigma_0}{2} f(-1 + T/T_0,\ X/D)|U|^2, \qquad 0 < X < L, \tag{3a}$$

where K is the thermal conductivity, ρ is the density, and C_p is the thermal capacity; each is piecewise constant on each slab. We also require that the temperature satisfies the surface heat balances

$$K \frac{\partial}{\partial X} = h(T - T_0) + se(T^4 - T_0^4), \qquad X = 0, \tag{3b}$$

$$-K \frac{\partial}{\partial X} = h(T - T_0) + se(T^4 - T_0^4), \qquad X = L, \tag{3c}$$

where h is the convective heat constant, s is the radiation heat constant, and e is the emissivity of the surface. Implicit in this model of surface heat transfer is the assumption that the sample sits in an infinite environment whose temperature is held fixed at T_0. This idealization is consistent with the assumption that the laminate is an infinite slab situated in an unbounded, homogeneous, and isotropic space.

Finally, we assume that the sample is initially at the ambient temperature,

$$T(X, 0) = T_0, \qquad 0 < X < L. \tag{3d}$$

The initial boundary value problem (2–3) constitutes the mathematical statement of the $\mathcal{P}$ problem.

We now state the $\mathcal{T}$ problem which parallels the above description. However, in this case, there are two type of incident polarization that are relevant. The first is the TM polarization where the electric field is aligned along the Z-axis. In the regions $X < 0$ and $X > L$ the field is given by

$$\mathbf{E} = E_0[\exp(\mathrm{i}k'X) + \sum_{m=-\infty}^{\infty} \Gamma_m \mathrm{e}^{2\pi \mathrm{i} m Y/D}\, \mathrm{e}^{-\mathrm{i}\beta_m X}]\hat{\mathbf{z}} \tag{4a}$$

and

$$\mathbf{E} = E_0[\sum_{m=-\infty}^{\infty} \Upsilon_m \mathrm{e}^{2\pi \mathrm{i} m Y/D}\, \mathrm{e}^{\mathrm{i}\beta_m X}]\hat{\mathbf{z}}, \tag{4b}$$

respectively, where the propagation constants β_m are given by

$$\beta_m = \sqrt{k'^2 - 4m^2\pi^2/D^2}. \tag{4c}$$

The terms in the infinite series represent modal solutions to the wave equation which possess the same periodic structure as the laminate. The reflection and transmission coefficients, Γ_m and Υ_m are to be determined.

In the laminate region,$0 < X < L$, $\mathbf{E} = E_0 U(X, Y)\hat{\mathbf{z}}$ where the dimensionless field U satisfies

$$\nabla^2 U + k'^2[N^2(Y/D) + \mathrm{i}\frac{\sigma_0}{\omega\epsilon_0} f(-1 + T/T_0,\ Y/D)]U = 0, \qquad 0 < X < L. \tag{4d}$$

Here N^2 and f are now piecewise constant functions of Y. The boundary conditions again are the continuity of the tangential electric and magnetic fields at the interface $X = 0$ and $X = L$.

These requirements are equivalent to the continuity of the electric field and its X derivative for this polarization.

The other relevant incident polarization is the TE case where the incident magnetic field is now aligned along the Z-axis. The magnetic field $\mathbf{H}$ is given in the exterior regions $X < 0$ and $X > L$ by (4a) and (4b), respectively, with $\mathbf{E}$ replaced by $\mathbf{H}$ and E_0 by H_0. In the laminate region, $0 < X < L$, $\mathbf{H} = H_0 V(X, Y)\hat{\mathbf{z}}$ where the dimensionless field V satisfies

$$\nabla \cdot \{\frac{1}{N^2 + i\sigma_0 f/\omega\epsilon_0} \nabla V\} + k'^2 V = 0, \tag{5a}$$

and where the arguments of N^2 and f are suppressed for notational convenience. These functions are again piecewise constant in the slabs.

For this polarization the electric field $\mathbf{E}$ in the laminate is obtained from Maxwell's equations and the vector form of $\mathbf{H}$; it is

$$\mathbf{E} = \frac{\mathrm{i}E_0}{k'[N^2 + \mathrm{i}\sigma_0 f/\omega\epsilon_0]}(V_Y\hat{\mathbf{x}} - V_X\hat{\mathbf{y}}). \tag{5b}$$

Finally, the boundary conditions again are the continuity of the tangential electric and magnetic fields at the interface $X = 0$ and $X = L$.

For both TM and TE incident polarizations of the microwave field the temperature T will depend upon both X and Y according to

$$\rho C_p \frac{\partial}{\partial t'} T = \nabla \cdot \{K \nabla T\} + E_0^2 \frac{\sigma_0}{2} f(-1 + T/T_0,\ Y/D)|\mathbf{E}|^2, \qquad 0 < X < L, \tag{6a}$$

where

$$|\mathbf{E}|^2 = E_0^2 \begin{cases} |U|^2 & \text{TM Case} \\ \dfrac{|V_X|^2 + |V_Y|^2}{k'^2|N^2 + \mathrm{i}\sigma_0 f/\omega\epsilon_0|^2} & \text{TE Case.} \end{cases} \tag{6b}$$

The boundary conditions are again given by (3b) and (3c), except now the effective heat-transfer coefficient h and the emissivity e are piecewise constant at the slab interfaces. The initial condition is again given by (3d). The initial-boundary-value problem (4) and (6) constitutes the mathematical statement of the $\mathcal{T}$ problem for TM polarization, and (5–6) for the TE polarization.

We shall now nondimensionalize our boundary-value problems and introduce certain dimensionless quantities which will play important roles. We begin by defining the dimensionless variables

$$(x, y) = (X, Y)/L, \quad W = -1 + T/T_0, \quad t = \frac{\rho_0 C_{p0} L^2}{K_0} t'$$

and the dimensionless parameters

$$B_0 = \frac{hL}{K_0}, \quad B_1 = \frac{seT_0^3}{h_0}, \quad k = k'L, \quad P = \frac{\sigma_0 L^2}{2T_0 K_0}|E_0|^2, \quad \delta = D/L,$$

and $\nu = \sigma_0/\omega\epsilon_0$, where ρ_0, C_{p0}, h_0, and K_0 are representative values of the density, the thermal capacity, the effective heat-transfer coefficient, and thermal conductivity, respectively, of SiC. Then the $\mathcal{P}$ problem (2–3) becomes

$$\frac{\mathrm{d}U}{\mathrm{d}x} + k^2[N^2(x/\delta) + \mathrm{i}\nu f(W,\ x/\delta)]U = 0, \qquad 0 < x < 1, \tag{7a}$$

$$\frac{\mathrm{d}U}{\mathrm{d}x} + \mathrm{i}kU = 2\mathrm{i}k, \qquad x = 0, \tag{7b}$$

$$\frac{\mathrm{d}U}{\mathrm{d}x} - \mathrm{i}kU = 0, \qquad x = 1, \tag{7c}$$

$$g(x/\delta)\frac{\partial}{\partial t}W = \frac{\partial}{\partial x}\{\kappa(x/\delta)\frac{\partial}{\partial x}W\} + Pf(W,\ x/\delta)|U|^2, \qquad 0 < x < 1, \tag{7d}$$

where $g(x/\delta) = \rho C_p/\rho_0 C_{p0}$ and $\kappa(x/\delta) = K/K_0$.

Finally, we also require that the temperature satisfies the surface heat balances

$$\kappa\frac{\partial}{\partial x}W = B_0\mathcal{L}(W), \qquad x = 0, \tag{7e}$$

$$-\kappa\frac{\partial}{\partial x}W = B_0\mathcal{L}(W) \qquad x = 1, \tag{7f}$$

$$\mathcal{L}(W) = lW + B_1 q[(1+W)^4 - 1], \tag{7g}$$

where l and q are constants which may have different values at $x = 0$ and 1, and the initial condition

$$W(x, 0) = 0, \qquad 0 < x < 1. \tag{7h}$$

The initial-boundary-value problem (7) constitutes the dimensionless mathematical statement of the $\mathcal{P}$ problem.

We shall now nondimensionalize the $\mathcal{T}$ problem along a similar path. We begin with TM polarization and set $\mathbf{e} = \mathbf{E}_0/E_0$. Then, since U is dimensionless already (4) becomes

$$\mathbf{e} = \hat{\mathbf{z}}\begin{cases} \mathrm{e}^{\mathrm{i}kx} + \displaystyle\sum_{m=-\infty}^{\infty} \Gamma_m \mathrm{e}^{2\pi\mathrm{i}my/\delta}\ \mathrm{e}^{-\mathrm{i}\beta_m x} & 0 < x, \\ \displaystyle\sum_{m=-\infty}^{\infty} \Upsilon_m \mathrm{e}^{2\pi\mathrm{i}my/\delta}\ \mathrm{e}^{\mathrm{i}\beta_m x} & x > 1, \end{cases} \tag{8a}$$

where now the propagation constant is given by the slightly modified form

$$\beta_m = \sqrt{k^2 - 4m^2\pi^2/\delta^2}. \tag{8b}$$

The equation for U, (4d), now becomes

$$\nabla^2 U + k^2[N^2(y/\delta) + \mathrm{i}\nu f(W,\ y/\delta)]U = 0, \qquad 0 < x < 1, \tag{8c}$$

where the Laplacian is in terms of x and y. The boundary conditions again are the continuity of the tangential electric and magnetic fields across the interfaces at $x = 0$ and 1.

For the TE polarization Equation (5) is replaced by

$$\nabla \cdot \{\frac{1}{N^2 + \mathrm{i}\nu f}\nabla V\} + k^2 V = 0, \tag{9a}$$

$$\mathbf{e} = \frac{\mathrm{i}}{k[N^2 + \mathrm{i}\nu f]}(V_y\hat{\mathbf{x}} - V_x\hat{\mathbf{y}}), \tag{9b}$$

where again the tangential electric and magnetic fields are continuous at $x = 0$ and 1. Finally, the heat equation (6) now becomes

$$g(y/\delta)\frac{\partial}{\partial t}W = \nabla \cdot \{\kappa(y/\delta)\nabla W\} + Pf(W, y/\delta)|\mathbf{e}|^2 \tag{10a}$$

where

$$|\mathbf{e}|^2 = \begin{cases} |U|^2 & \text{TM Case} \\ \dfrac{|V_x|^2 + |V_y|^2}{k^2|N^2 + \mathrm{i}\nu f|^2} & \text{TE Case.} \end{cases} \tag{10b}$$

The boundary conditions for W are again the surface heat balances

$$\kappa\frac{\partial}{\partial x}W = B_0\mathcal{L}_\delta(W), \qquad x = 0, \tag{10c}$$

$$-\kappa\frac{\partial}{\partial x}W = B_0\mathcal{L}_\delta(W), \qquad x = 1, \tag{10d}$$

$$\mathcal{L}_\delta(W) = l(y/\delta)W + B_1 q(y/\delta)[(1 + W)^4 - 1], \tag{10e}$$

where l and q are piecewise constant functions on each slab, and the initial condition is again (7g). The initial-boundary-value problem (8) and (10) constitute the dimensionless mathematical statement of the TM problem and (9–10), the TE problem.

Before ending this section we shall discuss the dimensionless parameters introduced above and pin down their sizes. The first dimensionless parameter is the fineness ratio of the structure $\delta = D/L$. We assume that the thickness of the slabs which make up the laminate are much smaller than the total thickness of the composite panel, *i.e.*, $\delta << 1$. This implies that the functions N^2, f, g, κ, l, and q are piecewise constant functions whose values rapidly change as one passes through each slab of the laminate. This will allow us to apply homogenization techniques to simplify the governing equations. The dimensionless wave number $k = k'L$ is assumed $O(1)$; this implies that the composite panel thickness is on the same order as the wavelength of the incident wave. For ceramic materials the parameters ν and β are relatively small [9,11,12], but we shall not exploit these facts here. Similarly, the Biot number B_0 is also small [11] and this will be used later after the equations have been smoothed. Finally, we assume the dimensionless power P is $O(1)$.

3. Asymptotic analyses

In this section we shall apply asymptotic methods to derive homogenized equations which describe the microwave heating of the laminate panels in the limit $\delta \to 0$. We use the method of multiple scales [13, Chapter 11] to do this for the $\mathcal{P}$ problem and a regular perturbation scheme for the $\mathcal{T}$ problem. Since both of these methods are well known, our presentation will be somewhat condensed.

3.1. THE $\mathcal{P}$ PROBLEM

Since the Equations (7) explicitly contain the variables $\eta \equiv x/\delta$ and x we seek an asymptotic solution of the form

$$U = u(\eta, x, t, \delta) = \sum_{n=0}^{\infty} \delta^n u_n(\eta, x, t), \tag{11a}$$

$$W = w(\eta, x, t, \delta) = \sum_{n=0}^{\infty} \delta^n w_n(\eta, x, t) \tag{11b}$$

as $\delta \to 0$. Inserting these expansions into (7), expanding the nonlinear terms using a Taylor series, and equating to zero the coefficients of the powers of δ, we obtain an infinite set of equations. These sequentially determine $u_n(\eta, x, t)$ and $w_n(\eta, x, t)$.

The leading-order $O(1)$ equations are

$$\frac{\partial^2}{\partial \eta^2} u_0 = 0, \qquad \frac{\partial}{\partial \eta}(\kappa(\eta)\frac{\partial}{\partial \eta} w_0) = 0 \tag{12a}$$

and their solutions are

$$u_0 = c_0(x, t) + \eta d_0(x, t) \quad \text{and} \quad w_0 = a_0(x, t) + b_0(x, t) \int_0^{\eta} \frac{1}{\kappa(\eta')} \, \mathrm{d}\eta', \tag{12b}$$

respectively. Now these solutions are required to be bounded as $\eta \to \infty$ and this clearly implies that $u_0 = c_0(x)$. We note also that this function satisfies the $O(1)$ boundary condition $\dfrac{\partial}{\partial \eta} u_0 = 0$. To make w_0 bounded, we first observe that the $\kappa(\eta)$ is a periodic function of η whose period is one. To see this observe that $\eta = x/\delta = x'/D$ and recall that K has period D. (See Figure 1a.) Then we note that the integral in (12b) becomes infinite as $\eta \to \infty$ and this clearly implies that $w_0 = a_0(x, t)$. This function also satisfies the $O(1)$ thermal boundary condition $\dfrac{\partial}{\partial \eta} w_0 = 0$ at $x = 0$. Finally, we shall not use a_0 and c_0, but rather $w_0(x, t)$ and $u_0(x, t)$ for notational convenience.

The order $O(\delta)$ equations are

$$\frac{\partial^2}{\partial \eta^2} u_1 = 0, \quad \frac{\partial}{\partial \eta}(\kappa \frac{\partial}{\partial \eta} w_1) + \kappa' \frac{\partial}{\partial x} w_0 = 0, \tag{13a}$$

where the prime denotes differentiation with respect to the argument of κ. The solutions of these equations are given by

$$u_1 = c_1(x, t) + \eta d_1(x, t), \quad w_1 = a_1(x, t) - \eta \frac{\partial}{\partial x} w_0 + b_1(x, t) \int_0^{\eta} \frac{1}{\kappa(\eta')} \, \mathrm{d}\eta'. \tag{13b}$$

The bounded solution of the first equation is again $u_1 = c_1(x, t)$. The $O(\delta)$ boundary conditions for u_1 are $u_{1\eta} + u_{0x} + \mathrm{i}k u_0 = 2\mathrm{i}k$ at $x = 0$ and $u_{1\eta} + u_{0x} - \mathrm{i}k u_0 = 0$ at $x = 1$. Since u_1 is a function only of x and t we obtain

$$\frac{\partial}{\partial x} u_0 + \mathrm{i}k u_0 = 2\mathrm{i}k, \qquad x = 0, \tag{14a}$$

$$\frac{\partial}{\partial x} u_0 - \mathrm{i}k u_0 = 0, \qquad x = 1. \tag{14b}$$

The second solution in (13b) remains bounded only when

$$\frac{\partial}{\partial x} w_0 = \hat{\kappa}^{-1} b_1(x,t) \tag{15a}$$

which follows by letting $\eta \to \infty$ through the positive integers. Here the constant $\hat{\kappa}$ is defined by

$$\hat{\kappa} = \frac{1}{\int_0^1 \frac{1}{\kappa}\,\mathrm{d}\eta} \equiv \frac{\kappa_1\kappa_2}{\alpha\kappa_2 + (1-\alpha)\kappa_1}, \tag{15b}$$

where κ_j is the dimensionless thermal conductivity in the j^{th} slab, $j = 1, 2$. Inserting (15a) into the second expression in (13b) gives

$$w_1 = a_1(x,t) + Q(\eta)\frac{\partial}{\partial x} w_0, \qquad Q(\eta) \equiv -\eta + \hat{\kappa}\int_0^\eta \frac{1}{\kappa(\eta')}\,\mathrm{d}\eta', \tag{15c}$$

where the function $Q(\eta)$ is periodic with period 1. The $O(\delta)$ boundary conditions for w_1 are $\kappa(w_{1\eta} + w_{0x}) + \mathcal{L}(w_0) = 0$ at $x = 0$ and $-\kappa(w_{1\eta} + w_{0x}) + \mathcal{L}(w_0) = 0$ at $x = 1$. Since it follows from (15c) that $\kappa(w_{1\eta} + w_{0x}) = \hat{\kappa} w_{0x}$, we deduce

$$-\hat{\kappa}\frac{\partial}{\partial x} w_0 + B_0\mathcal{L}(w_0) = 0, \qquad x = 0, \tag{16a}$$

$$\hat{\kappa}\frac{\partial}{\partial x} w_0 + B_0\mathcal{L}(w_0) = 0, \qquad x = 1. \tag{16b}$$

The final stage now is to obtain equations for u_0 and w_0. These come from the solvability conditions for the $O(\delta^2)$ equations which are

$$\frac{\partial^2}{\partial\eta^2} u_2 = -\{\frac{\partial^2}{\partial x^2} u_0 + k^2[N^2(\eta) + \mathrm{i}\nu f(w_0,\eta)]u_0\}, \tag{17a}$$

$$\frac{\partial}{\partial\eta}(\kappa\frac{\partial}{\partial\eta} w_2) = \{g(\eta)\frac{\partial}{\partial t} w_0 - \kappa(\eta)\frac{\partial^2}{\partial x^2} w_0 - Pf(w_0,\eta)|u_0|^2\} - \mathcal{M}(w_1), \tag{17b}$$

$$\mathcal{M}(w_1) = 2\kappa\frac{\partial^2 w_1}{\partial\eta\,\partial x} + \kappa'\frac{\partial}{\partial x} w_1. \tag{17c}$$

Integrating (17a) once with respect to η, we obtain

$$\frac{\partial}{\partial\eta} u_2 = -\{\eta\frac{\partial^2}{\partial x^2} u_0 + k^2[\int_0^\eta (N^2(\eta') + \mathrm{i}\nu f(w_0,\eta'))\,\mathrm{d}\eta']u_0\}.$$

For this to be bounded as $\eta \to \infty$ we demand that

$$\frac{\partial^2}{\partial x^2} u_0 + k^2[\hat{N}^2 + \mathrm{i}\nu\hat{f}(w_0)]u_0 = 0, \quad 0 < x < 1, \tag{18a}$$

where

$$\begin{aligned} \hat{N}^2 &= \int_0^1 N^2(\eta)\,\mathrm{d}\eta = \alpha N_1^2 + (1-\alpha)N_2^2, \\ \hat{f}(w_0) &= \int_0^1 f_{\mathcal{P}}(w_o,\eta)\,\mathrm{d}\eta = \alpha f_1(w_0) + (1-\alpha) f_2(w_0); \end{aligned} \tag{18b}$$

N_j^2 is the index of refraction and f_j the conductivity in the jth slab for $j = 1, 2$. This is our averaged equation for u_0.

The solvability condition for (17b) is somewhat more involved and is provided in Appendix A. The result is

$$\hat{g}\frac{\partial}{\partial t}w_0 = \hat{\kappa}\frac{\partial^2}{\partial x^2}w_0 + P\hat{f}_{\mathcal{P}}(w_0)|u_0|^2, \quad 0 < x < 1 \tag{19a}$$

where

$$\hat{g} = \int_0^1 g(\eta)\,\mathrm{d}\eta = \alpha g_1 + (1-\alpha)g_2. \tag{19b}$$

This our averaged equation for w_0.

Equations (18) and (19) along with their boundary conditions (14) and (16), respectively, and the initial condition $w_0 = 0$ constitute the averaged initial-boundary-value problem which will be attacked and studied in the next section.

3.2. The $\mathcal{T}$ problem

We begin this section with the analysis of the magnetic field in the TE polarization, *i.e.*, with an asymptotic analysis of (9a). There are two points to note before proceeding. First, we shall make explicit use of the piecewise character of the electrical properties. Secondly, we seek a regular expansion of V in the form

$$V(x, y, \delta) = v(x, \eta, \delta) = \sum_{n=0}^{\infty} \delta^n v_n(x, \eta), \tag{20}$$

where now $\eta = y/\delta = Y/D$. Since the incident wave striking the panel is independent of Y we require that V is periodic in Y with period D, or equivalently that v and all the v_n are periodic functions of η with period 1. We note here that a multiscale expansion similar to (11a) can be assumed and a similar analysis carried out. An averaged equation can be found whose solution depends upon x and y. However, this solution does not satisfy the boundary conditions at the interfaces $x = 0$ and $x = 1$. A boundary-layer analysis is required to fix this nonuniformity. The present approach is simpler and does not suffer this complication.

Before continuing forward with the determination of the v_n, we explicitly state the boundary conditions required at the material interfaces $\eta = 0$, α, and 1. First, the continuity of the z-component of the magnetic field requires $[v] = 0$, *i.e.*, v is continuous across these interfaces. This, of course, implies the same for all the v_n. Next, the continuity of the x-component of the electric field requires $[R\frac{\partial}{\partial \eta}v] = 0$, where $R = 1/[N^2 + \mathrm{i}\nu f]$, *i.e.*, $R\frac{\partial}{\partial \eta}v$ is continuous across each material interface. Secondly, since the v_n are periodic functions of η with period 1, we study the solutions of (9a) only for $0 < \eta < 1$. Thirdly, since there is no ambiguity in the values of v_n at each interface, the periodicity of the v_n implies $v_n(x, 0, t) = v_n(x, 1, t)$. Next, it is clear that periodicity requires $\frac{\partial}{\partial \eta}v_n(x, 1^+, t) = \frac{\partial}{\partial \eta}v_n(x, 0^+, t)$ where the $+$ denote values slightly above the interface. Using this and the fact that $R\frac{\partial}{\partial \eta}v_n$ is continuous across $x = 1$ we finally deduce

$$R(1^-)\frac{\partial}{\partial \eta}v_n(x, 1^-, t) = R(0^+)\frac{\partial}{\partial \eta}v_n(x, 0^+, t), \tag{21}$$

where the $-$ denotes values slightly below the interface.

We now insert (20) into (9a), expand the nonlinear terms using a Taylor series, and equate to zero the coefficients of the powers of δ to give an infinite set of equations. These sequentially determine the $v_n(x, \eta, t)$. The $O(1)$ equation is

$$\frac{\partial}{\partial \eta}(R\frac{\partial}{\partial \eta}v_0) = 0 \tag{22a}$$

whose solution is readily found to be

$$v_0 = a_0(x, t)\int_0^\eta \frac{1}{R}\,\mathrm{d}\eta + b_0(x, t). \tag{22b}$$

This function is clearly continuous across $\eta = \alpha$ and so is $R\frac{\partial}{\partial \eta}v_0 = a_0$. It must also be periodic, *i.e.*, $v_0(0) = v_0(1)$, which implies that $a_0 = 0$. Thus $v_0 = b_0$ is just a function of x and t. For notational ease we shall just refer to $v_0(x, t)$. It is then clear that v_0 automatically satisfies (21), too.

The $O(\delta)$ equation for v_1 is precisely (22a) and we deduce as above that it is a function of x and t. The $O(\delta^2)$ equation is

$$\frac{\partial}{\partial \eta}(R\frac{\partial}{\partial \eta}v_2) = -\{R(\eta)\frac{\partial^2}{\partial x^2}v_0 + k^2 v_0\} \tag{23a}$$

and integrating this once with respect to η, we have

$$R(\eta)\frac{\partial}{\partial \eta}v_2 = a_1(x, t) - \{\frac{\partial^2}{\partial x^2}v_0\int_0^\eta R(\eta')\,\mathrm{d}\eta' + k^2\eta v_0\} \tag{23b}$$

where $a_1(x, t)$ is unknown at this stage. Now it is clear from this result that $R\frac{\partial}{\partial \eta}v_2$ is continuous across $\eta = \alpha$. The application of the periodicity condition (21) leads to our new averaged equation

$$\frac{\partial^2}{\partial x^2}v_0 + k^2\hat{N}^2 v_0 = 0, \quad 0 < x < 1, \tag{24a}$$

where now

$$\hat{N}^2 = \frac{1}{\int_0^1 R(\eta)\,\mathrm{d}\eta} = \frac{(N_1^2 + \mathrm{i}\nu f_1)(N_2^2 + \mathrm{i}\nu f_2)}{\alpha(N_2^2 + \mathrm{i}\nu f_2) + (1-\alpha)(N_1^2 + \mathrm{i}\nu f_1)}. \tag{24b}$$

The evaluation of the integral in (24b) anticipates the fact that the temperature, to leading order, is independent of η. Now, Equation (23b) can be further integrated to determine v_2 up to a single unknown function of x and t, but we shall not do so here. Finally, the electric field corresponding to v_0 is obtained from (9b); it is

$$\mathbf{e} = -\frac{\mathrm{i}R}{k}\frac{\partial}{\partial x}v_0\hat{\mathbf{y}}. \tag{25}$$

The differential equation (24a) requires two pieces of boundary data which we shall now derive. First, we recall that the dimensionless magnetic field $\mathbf{h}$ in the regions $x < 0$ and $x > 1$ are given by (8a) with $\mathbf{e}$ replaced by $\mathbf{h}$. Then at $x = 0$ the continuity of this field implies

$$v(0, \eta, t) = 1 + \sum_{m=-\infty}^{\infty} \Gamma_m \mathrm{e}^{2\pi \mathrm{i} m \eta},$$

where we have replaced y/δ by η. This relationship holds true for $0 < \eta < 1$. Now we expand v on the left-hand side of this expression according to (20) and also introduce a power series expansion of Γ. Equating the leading-order $O(1)$ terms gives

$$v_0(0, t) = 1 + \sum_{m=-\infty}^{\infty} \Gamma_m^0 \mathrm{e}^{2\pi \mathrm{i} m \eta}, \tag{26a}$$

where Γ_m^0 is the leading term in the Γ expansion.

Now, the tangential component of the electric field must be continuous across $x = 0$. In the region $x < 0$ it is given by $\dfrac{-\mathrm{i}}{k} \dfrac{\partial}{\partial x} \mathbf{h} \cdot \hat{\mathbf{y}}$ where we use the fact $R = 1$ in free space. In the region $0 < x < 1$ it is given to leading order by (25). Equating these two relationships gives to leading order

$$R \frac{\partial}{\partial x} v_0(0, t) = \mathrm{i}k - \mathrm{i} \sum_{m=-\infty}^{\infty} \beta_m \Gamma_m^0 \mathrm{e}^{2\pi \mathrm{i} m \eta}. \tag{26b}$$

Finally, integrating (26a) and (26b) with respect to η from 0 to 1, we obtain $v_0 = 1 + \Gamma_0^0$ and $\hat{R} v_{0x} = \mathrm{i}k(1 - {\Gamma_0}^0)$, respectively, where $\hat{R} = 1/\hat{N}^2$ and $\beta_0 = k$. Elimination of ${\Gamma_0}^0$ from these expressions yields

$$\frac{\partial}{\partial x} v_0 + \mathrm{i}k\hat{N}^2 v_0 = 2\mathrm{i}k\hat{N}^2, \quad x = 0. \tag{27a}$$

A similar analysis done at $x = 1$ gives

$$\frac{\partial}{\partial x} v_0 - \mathrm{i}k\hat{N}^2 v_0 = 0, \quad x = 1. \tag{27b}$$

Equations (24) and (27) constitute the electromagnetic equations and boundary conditions for TE polarization.

The asymptotic analysis for the electric field in the TM polarization case follows along exactly the same lines. The only difference is that the dimensionless electric field U is continuous and its normal derivative across a material interface is too. Thus, the function R will not appear in any of the boundary calculations. For sake of brevity we simply state the results here. They are $U \sim u_0(x, t)$ where u_0 satisfies precisely Equation (18) and the boundary conditions (14).

We finish this section with an analysis of the thermal portion of the $\mathcal{T}$ problem, *i.e.*, an asymptotic analysis of (10). Following a similar path to the one above we seek a regular expansion of W in the form

$$W(x, y, \delta) = w(x, \eta, \delta) = \sum_{n=0}^{\infty} \delta^n w_n(x, \eta). \tag{28}$$

Since the electric field is periodic in η, the source term in the heat equation is too. Thus, we require that w and the w_n are periodic functions of η with period 1. The temperature is continuous across the material interfaces and thus, so are the w_n. The thermal flux $\kappa \dfrac{\partial}{\partial \eta} w$ are also required to be continuous across material interfaces. This, the periodicity of w, and the same reasoning used to deduce (21) yield

$$\kappa(1^-)\frac{\partial}{\partial\eta}w_n(x,1^-,t)=\kappa(0^+)\frac{\partial}{\partial\eta}w_n(x,0^+,t). \tag{29}$$

We now insert (28) into (10a) and go through the same process. Skipping the calculations, as they are very similar to those used to deduce v_0, we find that w_0 and w_1 are functions only of x and t. Proceeding forward we find that the $O(\delta^2)$ equation becomes

$$\frac{\partial}{\partial\eta}(\kappa\frac{\partial}{\partial\eta}w_2)=g(\eta)\frac{\partial}{\partial t}w_0-\{\kappa\frac{\partial^2}{\partial x^2}w_0+Pf(w_0,\eta)|\mathbf{e}(x,t)|^2\} \tag{30}$$

where $\mathbf{e}$ is given by (25) for TE incident polarization and by $u_0\hat{z}$ for TM polarization. Integrating (30) once with respect to η and demanding (29) yields for the TE case

$$\hat{g}\frac{\partial}{\partial t}w_0=\hat{\kappa}\frac{\partial^2}{\partial x^2}w_0+\frac{P}{k^2}\{\frac{\alpha f_1(w_0)}{N_1^4+\nu^2f_1^2(w_0)}+\frac{(1-\alpha)f_2(w_0)}{N_2^4+\nu^2f_2^2(w_0)}\}|v_{ox}|^2, \tag{31a}$$

where $\hat{g}$ is given by (19b) and $\hat{\kappa}$ is now given by

$$\hat{\kappa}=\int_0^1\kappa\,\mathrm{d}\eta=\alpha\kappa_1+(1-\alpha)\kappa_2. \tag{31b}$$

For the TM case we obtain exactly (19a) with $\hat{\kappa}$ given by (31b).

The leading-order approximation w_0 is a function of x and t. If the dimensionless heat-transfer function l and radiative function q contained in the boundary condition (10) are constant, *i.e.*, they are not material-dependent, then w_0 also satisfies (16). On the other hand, if they are not constant, then the boundary conditions given in (10) depend upon η. This implies that w_0 is not a uniform approximation to w in x. We have performed a boundary-layer analysis near $x=0$ and $x=1$ to remove this nonuniformity, but omit the details here for brevity. The results of this analysis lead to the averaged boundary conditions

$$-\hat{\kappa}\frac{\partial}{\partial x}w_0+B_0\hat{\mathcal{L}}(w_0)=0,\quad x=0, \tag{31c}$$

$$\hat{\kappa}\frac{\partial}{\partial x}w_0+B_0\hat{\mathcal{L}}(w_0)=0,\quad x=1, \tag{31d}$$

where

$$\hat{\mathcal{L}}(w_0)=\hat{l}w_0+B_1\hat{q}\{(w_0+1)^4-1\}, \tag{31e}$$

$$\hat{l}=\alpha l_1+(1-\alpha)l_2,\quad \hat{q}=\alpha q_1+(1-\alpha)q_2. \tag{31f}$$

4. Small Biot-number-analyses

We begin this section by considering the $\mathcal{P}$ problem which is restated here for convenience as

$$\hat{g}\frac{\partial}{\partial t}w_0=\hat{\kappa}\frac{\partial^2}{\partial x^2}w_0+P\hat{f}(w_0)|u_0|^2,\quad 0<x<1, \tag{32a}$$

$$-\hat{\kappa}\frac{\partial}{\partial x}w_0+B_0\mathcal{L}_1(w_0)=0,\qquad x=0, \tag{32b}$$

$$\hat{\kappa}\frac{\partial}{\partial x}w_0 + B_0\mathcal{L}_2(w_0) = 0, \qquad x = 1, \tag{32c}$$

$$w_0(x, 0) = 0, \qquad 0 < x < 1. \tag{32d}$$

$$\frac{\partial^2}{\partial x^2}u_0 + k^2[\hat{N}^2 + \mathrm{i}\nu\hat{f}(w_0)]u_0 = 0, \quad 0 < x < 1, \tag{33a}$$

$$\frac{\partial}{\partial x}u_0 + \mathrm{i}ku_0 = 2\mathrm{i}k, \qquad x = 0, \tag{33b}$$

$$\frac{\partial}{\partial x}u_0 - \mathrm{i}ku_0 = 0, \qquad x = 1, \tag{33c}$$

where $\hat{g}$, $\hat{\kappa}$, $\hat{f}$ and $\hat{N}^2$ are defined by (19b), (15b), and (18b), respectively. The subscripts on the boundary operator $\mathcal{L}$ denote the possibility that the first and last slabs in the laminate are made of different materials.

In many applications the Biot number B_0 is small and this has been exploited [9,11,12] to determine an asymptotic approximation of the solutions to (32–33). Following this analysis we introduce a slow time variable $\tau = B_0 t$ and a rescaled dimensionless power parameter $p = P/B_0$, where $p = O(1)$. This new time scale allows us to study the heating process on a long time scale that is dictated by the small heat loss on the boundaries $x = 0$ and 1. The functions w_0 and u_0 are then expanded in a power series in B_0 and this yields in the usual fashion a infinite number of equations that must be solved sequentially. To leading order the calculation shows that w_0 is a function only of τ, but u_0 depends on both independent variables. A solvability condition is applied at the next order and this gives

$$\hat{g}\frac{\mathrm{d}w_0}{\mathrm{d}\tau} = -\{\mathcal{L}_1(w_0) + \mathcal{L}_2(w_0)\} + p\hat{f}(w_0)||u_0||^2, \tag{34a}$$

$$||u_0||^2 \equiv \int_0^1 |u_0|^2\,\mathrm{d}x, \tag{34b}$$

$$w_0(0) = 0. \tag{34c}$$

In these equations w_0 and u_0 denote the leading-order terms in the Biot-number expansion. Accordingly, the function u_0 determined by (33) depends upon τ parametrically through $\hat{f}(w_0)$. It is interesting to observe at this point that the effective thermal conductivity $\hat{\kappa}$ plays no role at this stage.

The problem now is to solve (33) and (34). Since u_0 depends only upon τ parametrically, an explicit solution to (33) can be obtained; it is

$$u_0 = A\,\exp(\mathrm{i}Kx) + B\,\exp(-\mathrm{i}Kx), \tag{35a}$$

where K, A, and B are defined by

$$K(\tau) = k\sqrt{\hat{N}^2 + \mathrm{i}\nu\hat{f}(w_0)}, \tag{35b}$$

$$A(\tau) = \frac{-2k(K + k)}{\Delta}\exp(-\mathrm{i}K), \tag{35c}$$

$$B(\tau) = \frac{-2k(K-k)}{\Delta}\exp(+\mathrm{i}K), \tag{35d}$$

$$\Delta(\tau) = (K-k)^2\exp(\mathrm{i}K) - (K+k)^2\exp(-\mathrm{i}K). \tag{35e}$$

Substituting (35a) in (34b), performing the integration, and inserting the resulting expression into (34a) yields an ordinary differential equation for w_0. This equation, along with the initial condition (34c) must in general be solved numerically. However, the steady-state temperature w_0^* is implicitly given by

$$p = \frac{\mathcal{L}_1(w_0^*) + \mathcal{L}_2(w_0^*)}{\hat{f}(w_0^*)||u_0||^2(w_0^*)}. \tag{36}$$

This will be studied shortly.

We now attack the $\mathcal{T}$ problem using the same approach. We begin with the case of TM polarization and find that w_0 and u_0 are again described by (33–34) with two minor changes; the constant $\hat{\kappa}$ is now given by (31b) and the boundary operators $\mathcal{L}_j(w_0)$ are each replaced by $\hat{\mathcal{L}}(w_0)$ defined in (31e–f). Performing the small-Biot-number approximation yields with these changes precisely (34–36). In particular the steady-state temperature w_0^* is now given implicitly by

$$p = \frac{2\hat{\mathcal{L}}(w_0^*)}{\hat{f}(w_0^*)||u_0||^2(w_0^*)}, \tag{37}$$

where again $\hat{\kappa}$ is again plays no role at this stage.

Finally, we tackle the TE polarization using the same approach. We find that w_0 again satisfies (32) with two exceptions. The first was given above; the boundary operators $\mathcal{L}_j(w_0)$ are each replaced by $\hat{\mathcal{L}}(w_0)$. The second is the source term in (32a); $|u_0|$ is replaced by $|\mathbf{e}|$ where $\mathbf{e}$ is defined in (25). The small-Biot-number analysis then gives

$$\hat{g}\frac{\mathrm{d}w_0}{\mathrm{d}\tau} = -2\hat{\mathcal{L}}(w_0) + \frac{p}{k^2}\{\frac{\alpha f_1(w_0)}{N_1^4 + \nu^2 f_1^2(w_0)} + \frac{(1-\alpha)f_2(w_0)}{N_2^4 + \nu^2 f_2^2(w_0)}\}||v_{0x}||^2, \tag{38a}$$

$$||v_{0x}||^2 = \int_0^1 |v_{0x}|^2\,\mathrm{d}x. \tag{38b}$$

In Equation (38) the function v_0 satisfies (24) with boundary conditions (27). These are slightly different from (33), but the solution can be obtained in a similar fashion. The result is

$$v_0 = A\,\exp(\mathrm{i}Kx) + B\,\exp(-\mathrm{i}Kx) \tag{39a}$$

where K, A, and B are now defined by

$$K(\tau) = k\hat{N}, \tag{39b}$$

$$A(\tau) = \frac{-2K(K+k)}{\Delta}\exp(-\mathrm{i}K), \tag{39c}$$

$$B(\tau) = \frac{-2K(k-K)}{\Delta}\exp(+\mathrm{i}K), \tag{39d}$$

$$\Delta(\tau) = (K-k)^2 \exp(\mathrm{i}K) - (K+k)^2 \exp(-\mathrm{i}K), \tag{39e}$$

where $\hat{N}^2$ is given by (24b). Finally, the steady-state temperature w_0^* is now given implicitly by

$$p = \frac{2k^2 \hat{\mathcal{L}}(w_0^*)}{S(w_0)||v_{0x}||^2(w_0^*)}, \tag{40a}$$

$$S(w_0) = \frac{\alpha f_1(w_0)}{N_1^4 + \nu^2 f_1^2(w_0)} + \frac{(1-\alpha) f_2(w_0)}{N_2^4 + \nu^2 f_2^2(w_0)}. \tag{40b}$$

5. Numerical experiments and discussion

We now apply our theories to the two chemical-vapor applications described in the introduction. The first deals with the fabrication of a SiC composite panel and is mathematically moedled as the $\mathcal{P}$ problem which is described by Equations (14), (18), and (19). The second deals with heating a porous slab and is mathematically modeled as the $\mathcal{T}$ problem which is described by Equations (24), (27), and (21). We numerically approximate the steady-state solutions to these two problems using a standard second-order finite-difference scheme. This yields an algebraic system for the temperature and electric (or magnetic) field values. We then apply standard continuation techniques to determine the relationship between the applied power and the temperature. We used three hundred grid points over the domain $0 \leq x \leq 1$ to produce approximates to the temperature and produced approximations to the temperature and electromagnetic fields that were accurate within 1%. This method produces accurate methods, regardless of the size of the Biot number. Finally, we compare these numerical approximations against the results of the small Biot number theory which are given by (36), (37) and (40).

For the $\mathcal{P}$ problem, we investigate a simplified structure that is motivated by the CVI experiments found in Jaglin *et al.* [2]. The composite panel is constructed from two type of SiC sheets. The first is a fibrous sheet composed of SiC fibers. The second is the same sheet, except it has been embedded with carbon particles to enhance the electrical conductivity. Sheets of the first type are layered to produce a laminate which occupies the region $0 < X < \alpha D$. Sheets of the second type are layered to produce the laminate which occupies the region $\alpha D < X < D$. This composition is then repeated to build up the composite panel.

To estimate the physical properties of the first sheet, we use a mixture theory assuming that the material properties of the fabric are functions of the volume fraction of SiC in the fabric. Typical values of volume fraction are near 50%, and we simply divide the scaled material properties of SiC by two. In the second sheet, we assume the embedded particles completely fill the voids and take its material properties to be identical to SiC. In addition, we assume that the effective heat transfer of the two laminates are the same. The resulting nondimensional quantities are shown in the first column of Table 1 where we have assumed that the characteristic electrical conductivity is that of SiC at room temperature.

Figure 2 shows the temperature $w_0(0)$ plotted against the input power $p = P/B_0$ for two different values of the Biot number B_0. The solid curves are the results of our finite difference calculations, while the dots on these curves correspond to the small-Biot-number result (36). The solid lines correspond to $\alpha = 0{\cdot}1$, *i.e.*, 10 percent of the laminate is composed of sheets of the first type and 90 percent of the second type, the dashed lines correspond to $\alpha = 0{\cdot}4$, the dashed-dotted lines correspond to $\alpha = 0{\cdot}6$, and the fine dotted lines correspond to $\alpha = 0{\cdot}9$.

Table 1. Dimensionless parameters for each of the systems considered.

Parameter	Fabric-layers [2]	H_2 filled pores [5]
N_1^2	5	1
N_2^2	10	10
ν	0·01	0·01
k	1	1
f_1	$\frac{1}{2}\exp(3w_0)$	0
f_2	$\exp(3w_0)$	$\exp(3w_0)$
κ	2	200
B_1	10^{-4}	10^{-4}

We observe several interesting results from these curves. First, more power is required to reach a prescribed $w_0(0)$ as α is increased. This is because the effective electrical conductivity of the composite panel decreases as α increases, *i.e.*, as more of the fibrous sheets are used to build the laminate. Second, the curves show the familiar S-shaped response found for solid slabs [11]. The lower branch of this curve corresponds to a balance between the microwave power put into the structure and the heat lost at is surfaces. As the power is increased passed a critical point this balance is lost; the surfaces can not dissipate the required power. As the temperature rises, the effective electrical conductivity of the composite panel increases and this causes the skin effect which reduces the electric field in the panel. This reduction limits the power and produces the upper branch. This is again borne out in Figure 2. For a fixed power level, the upper branch decreases as α decreases and the composite panel becomes electrically more conductive. This exacerbates the skin effect and reduces the final temperature. Finally, we observe that for these values of B_0, the small-Biot-number approximation yields excellent agreement with our numerical simulations.

Figure 3 shows the deviation of the temperature $w_0(x)$ from its mean value $\bar{w}_0 = \int_0^1 w_0(x)\,\mathrm{d}x$ and the electric field from its mean value given by (34b) for $B_0 = 0{\cdot}01$, $\alpha = 0{\cdot}9$, and $p = 0{\cdot}5$. From Figure 2 we see that this value of p yields solutions on the lower and upper branches. The solid curves in Figure 3 correspond to the lower branch solution and the dotted curves to the upper branch. There are two interesting observations to be made at this point. First, the temperature on the lower branch is essentially the constant given by the corresponding graph in Figure 2. The electric field on the other hand oscillates about its mean. Secondly, the roles are reversed for the upper branch solution. The temperature now varies by about ten percent from its mean value and the electric field is essentially a constant, except for a small interval near $x = 0$. This localization is the skin effect.

Now we consider the $\mathcal{T}$ problem. As a physical example, we consider a periodic structure composed of a SiC layers separated by pores filled with inert H_2 gas. Within the fundamental cell the gas occupies the region $0 < Y < \alpha D$, and the solid the region $\alpha D < Y < D$. This system is a two-dimensional extension of the problem considered in reference [5], where the authors considered only one circular pore. This assumption, as well as taking a temperature independent electrical conductivity, decouples the wave equation from the heat equation. Although our structure is two-dimensional, it takes both of these features into account. The nondimensional parameters for this system are found in the second column of Table 1.

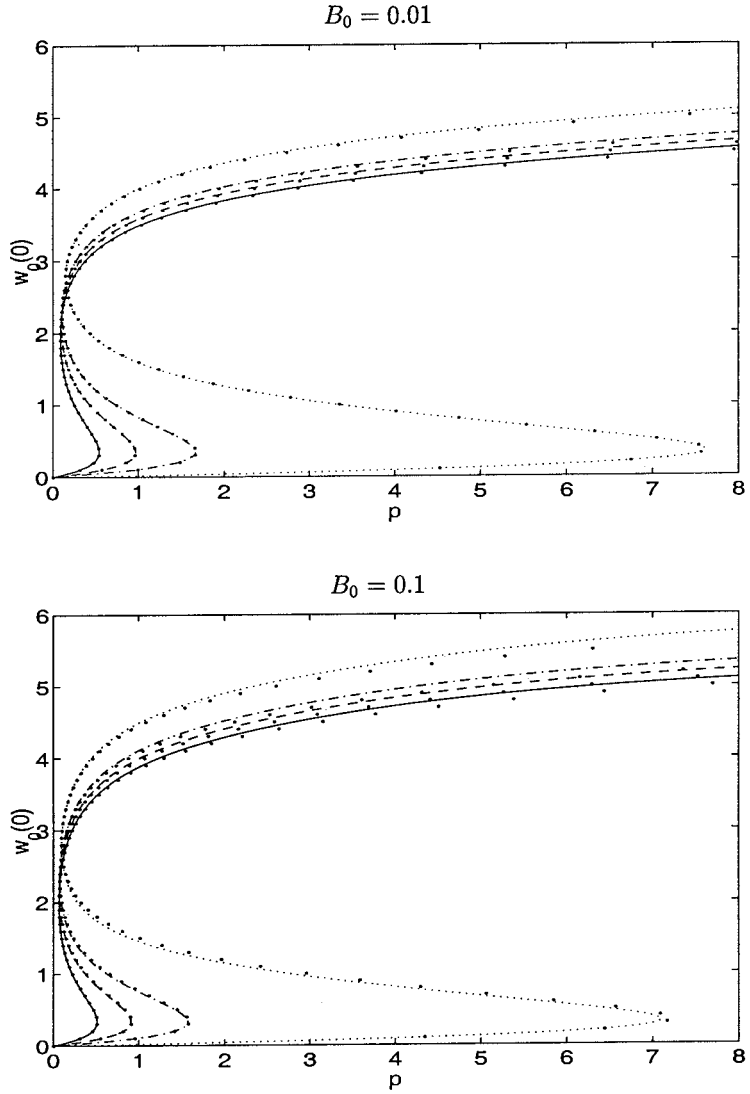

Figure 2. Plots of temperatures $w_o(0)$ for different power levels p at different Biot numbers $B_0 = 0{\cdot}01$ and $B = 0{\cdot}1$ in the P configuration. Lines correspond to the solution of the full system with the solid curves corresponding to $\alpha = 0{\cdot}1$, dashed curves corresponding to $\alpha = 0{\cdot}4$, dashed-dot curves corresponding to $\alpha = 0{\cdot}6$, and dotted curves corresponding to $\alpha = 0{\cdot}9$. The solid dots on the curves are the approximations using the small-Biot-number analysis in Equation (36).

First we consider the TM polarization. Figure 4 shows the corresponding S-shaped curves in this physical situation for Biot numbers $B_0 = 0{\cdot}01$ and $B_0 = 0{\cdot}1$. Solid lines correspond to $\alpha = 0{\cdot}1$ (10% volume fraction of the pore), dashed lines correspond to $\alpha = 0{\cdot}4$, dashed-dotted lines correspond to $\alpha = 0{\cdot}6$, and fine dotted lines correspond to $\alpha = 0{\cdot}9$. We note again that as the amount of SiC in the structure decreases, larger power levels are required to reach a prescribed temperature. Similarly, we observe that increasing the amount of SiC in the structure lowers the temperature on the upper branch for a given power level. In all cases, the small-Biot-number approximations, given by the individual dots, are in excellent agreement with our numerical simulations.

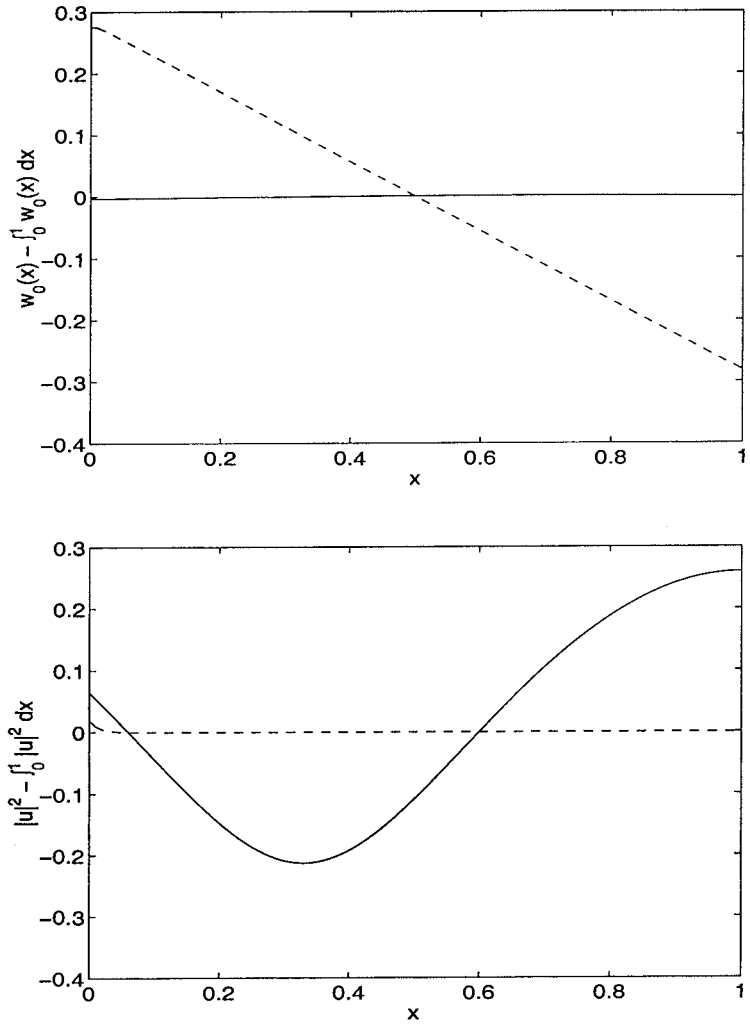

Figure 3. Plots of temperature profiles (upper figure) and electric field-strengths (lower figure) at $p = 0{\cdot}5$ for $\alpha = 0{\cdot}9$ for the lower branch (solid curve) and the upper branch (dashed line). The both are plotted as the deviation from the average value. Notice that the temperature deviation is indicative of the electric-field strength.

In Figure 5, we plot the deviation of the temperature $w_0(x)$ from its mean value $\bar{w}_0$ and $|u_0|^2$ for $p = 1{\cdot}0$ and $\alpha = 0{\cdot}4$, where the solid lines correspond to the lower branch of the S-shaped curve, while the dotted lines correspond to the upper branch. We observe that the temperature is nearly uniform on the lower branch and the electric-field strength exhibits behavior typical of a lossless medium. Along the upper branch, however, the electric field strength is again nearly zero, except for a small interval near $x = 0$; this is again the skin effect. In addition, the very small value of the electric field in the interior of the structure essentially shuts off the source term in the effective heat equations. This produces a nearly linear temperature profile in this region and this is borne out in Figure 5.

We now consider the TE polarization. Figure 6 shows the corresponding S-shaped curves in this physical situation for Biot numbers $B_0 = 0{\cdot}01$ and $B_0 = 0{\cdot}1$. Again, the solid lines correspond to $\alpha = 0{\cdot}1$, the dashed to $\alpha = 0{\cdot}4$, the dashed-dotted to $\alpha = 0{\cdot}6$, and the fine dotted to $\alpha = 0{\cdot}9$. There are two interesting observations to be made at this point, each

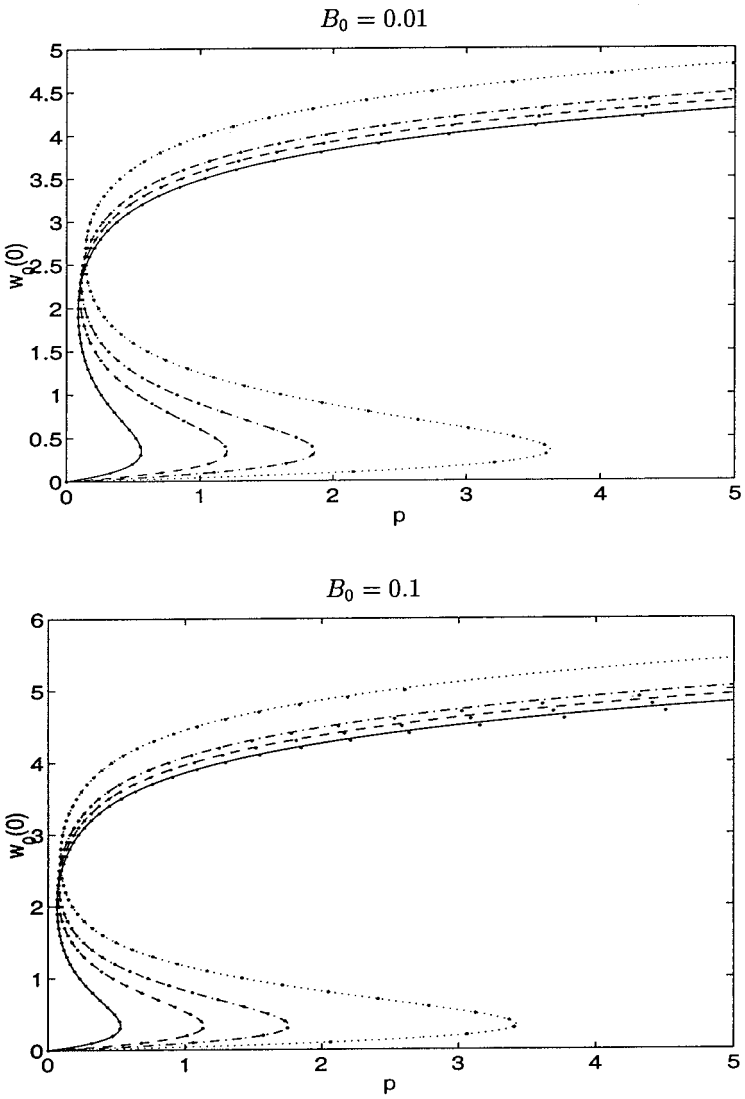

Figure 4. Plots of temperatures $w_o(0)$ for different power levels p at different Biot numbers $B_0 = 0{\cdot}01$ and $B = 0{\cdot}1$ in the TM polarization for the T orientation. Lines correspond to the solution of the full system with the solid curves corresponding to $\alpha = 0{\cdot}1$, dashed curves corresponding to $\alpha = 0{\cdot}4$, dashed-dot curves corresponding to $\alpha = 0{\cdot}6$, and dotted curves corresponding to $\alpha = 0{\cdot}9$. The solid dots on the curves are the approximations using the small-Biot-number analysis in Equation (37).

contrasting the difference between the TM and TE polarizations. These differences are seen by comparing Figures 4 and 6. First, for a given value of α more power is required to reach a prescribed temperature in the TE case. This is trend is clearly borne out when considering the critical power. For example, if we take $\alpha = 0{\cdot}1$ and $B_0 = 0{\cdot}1$, then from Figure 4 the critical power for the TE polarization is $\sim 0{\cdot}5$; for the same α and B_0 the critical power for the TE case is $\sim 3{\cdot}0$. The second observation is for a given p, α and B_0, the temperature on the upper branch for the TE polarization is less than the corresponding value for the TM case. For example, if we take $p = 1$, $B_0 = 0{\cdot}1$, and $\alpha = 0{\cdot}4$, then from Figure 4 the temperature on the upper branch is $\sim 3{\cdot}75$; the for the same parameters, the corresponding temperature in

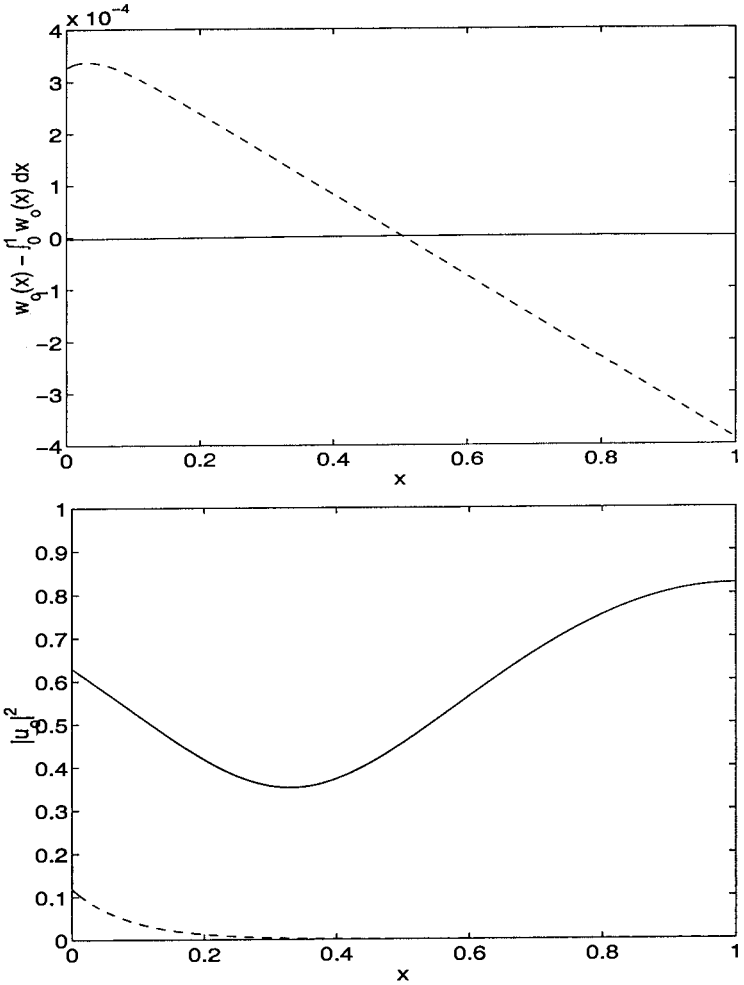

Figure 5. Plots of temperature profiles $w_0(x) - \bar{w}_0$ and the electric-field distribution $|u_0|^2$ for $B_0 = 0{\cdot}01$ in the T orientation with $\alpha = 0{\cdot}5$ for $p = 1$. Solid curves correspond to profiles on the lower branch of the S-shaped curve, while dashed lines correspond to upper branch profiles.

the TE case is $\sim 2{\cdot}6$. Both these observations indicate that the electromagnetic fields couple more strongly to the composite panel in the TM case.

Figure 7 shows the deviation of the temperature $w_0(x)$ from its mean value $\bar{w}_0$ and $|\mathbf{e}|^2$ for $\alpha = 0{\cdot}1$, $p = 2$, and $B_0 = 0{\cdot}1$. Again, the solid curves correspond to the lower branch and the dashed curves to the upper branch. The results for the lower branch are qualitatively similar to those for the TM case. However, the behavior on the upper branch is different. First, we note that the electric field intensity does not exhibit the typical skin effect at $x = 0$, but is small throughout the interior of the structure. This can be understood by examining the effective index of refraction $\hat{N}^2$ given by Equation (24b). Setting $f_1 = 0$ and $N_1^2 = 1$ for this physical application we obtain

$$\hat{N}^2 = \frac{N_2^2 + \mathrm{i}\nu f_2}{(1-\alpha) + \alpha(N_2^2 + \mathrm{i}\nu f_2)}. \tag{41}$$

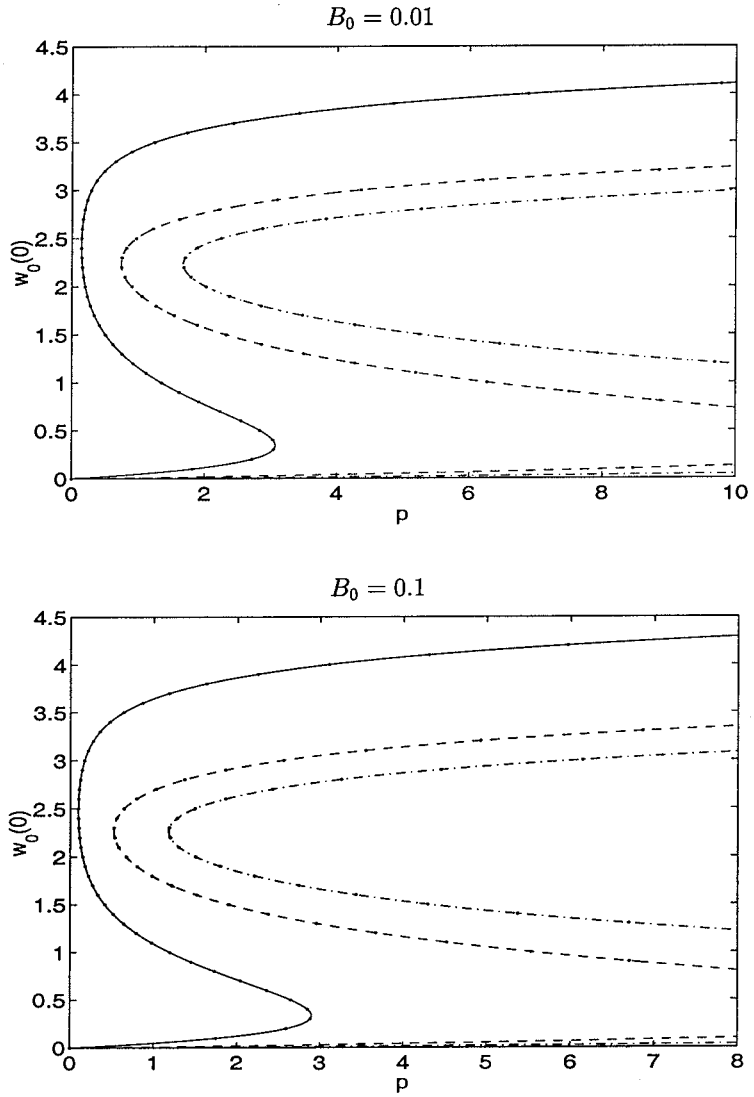

Figure 6. Plots of temperatures $w_o(0)$ for different power levels p at different Biot numbers $B_0 = 0{\cdot}01$ and $B = 0{\cdot}1$ in the TE polarization for the T orientation. Lines correspond to the solution of the full system with the solid curves corresponding to $\alpha = 0{\cdot}1$, dashed curves corresponding to $\alpha = 0{\cdot}4$, dashed-dot curves corresponding to $\alpha = 0{\cdot}6$, and dotted curves corresponding to $\alpha = 0{\cdot}9$. The solid dots on the curves are the approximations using the small-Biot-number analysis in Equation (37).

On the upper branch $f_2 >> 1$ and this makes $\hat{N}_2^2 \sim 1/\alpha^2$, which clearly diminishes the skin effect, since this depends upon the imaginary part of $\hat{N}^2$.

Finally, we observe that the temperature profile on the upper branch is slightly warmer in the center of the structure and symmetric. The latter feature stems from the symmetry of $|\mathbf{e}|^2$ as shown in Figure 7. And the former behavior suggests that the TE polarization may be more useful than the TM in the CVI process where a hotter center region would cause the composite to form from the interior to the exterior [1].

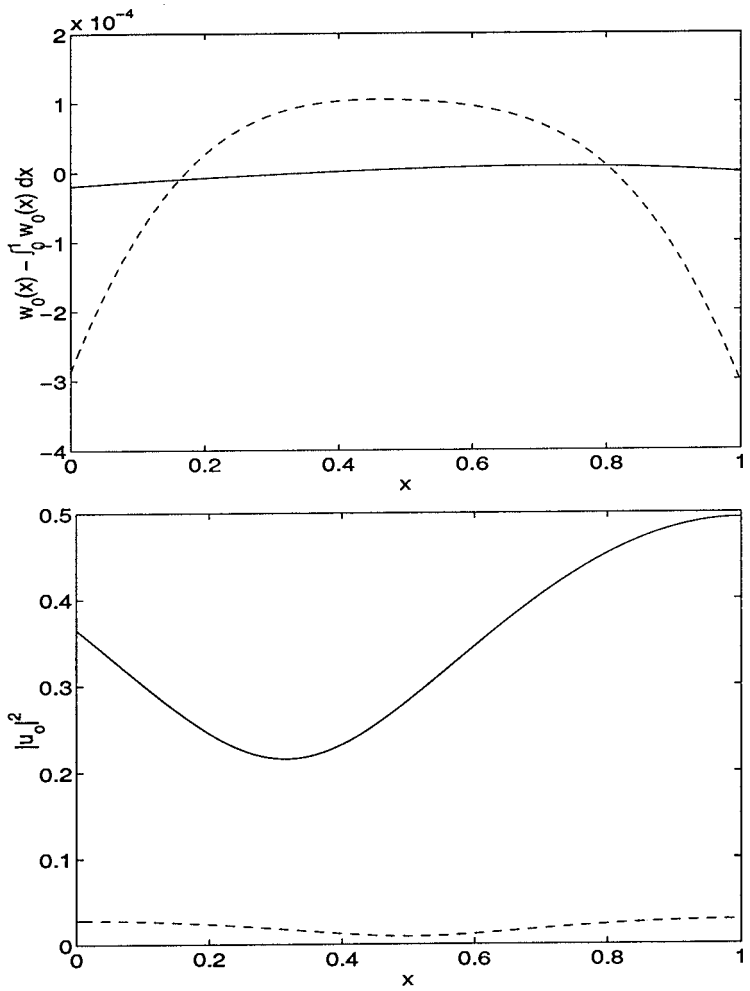

Figure 7. Plots of temperature profiles $w_0(x) - \bar{w_0}$ and the electric-field intensity $|\mathbf{e}|^2$ for $B_0 = 0{\cdot}1$ for the T orientation with $\alpha = 0{\cdot}1$ for $p = 2$. Solid curves correspond to profiles on the lower branch of the S-shaped curve, while dashed lines correspond to upper branch profiles.

6. Conclusions

In this paper we have studied the microwave heating of two different composite panels. In the first, the $\mathcal{P}$ problem we used multiple scale analysis to systematically derive averaged wave and heat equations. The solutions of these equations were approximated using finite differences and these results were compared to those obtained from a small-Biot-number analysis. The agreement was excellent for Biot numbers $\sim 0{\cdot}1$. More importantly, we were able to establish trends between the steady-state temperature and the physical properties of the laminates which make up the panel.

In the $\mathcal{T}$ problem we used a variation of slender-body theory to systematically derive the averaged wave and heat equations. These equations are almost identical to those of the $\mathcal{P}$ problem for TM incident microwaves; only the effective thermal conductivity is different. However, in the case of TE polarization the equations are somewhat different. The averaged wave equation now has a more complicated effective index of refraction. In addition to a mod-

ified effective thermal conductivity, the heat equation has a significantly different source term. This source term has an important consequence in the microwave heating of this structure. Specifically, we have shown through our numerical simulations that far more power is required to heat the panel for this polarization than the TM. However, our simulations also show that the thermal gradients are larger in this case than the TM. This suggests that, although the TE polarization is less efficient in heating the slab, the gradients may in fact be more conducive to CVI processes.

Appendix A

In this appendix we consider the solvability condition for (17b−17c) and deduce the averaged equation (19). We begin by combining (15c) and (17c) to obtain

$$\mathcal{M}(w_1) = 2\kappa \frac{\mathrm{d}Q}{\mathrm{d}\eta}\frac{\partial^2}{\partial x^2}w_0 + \kappa'[\frac{\partial}{\partial x}a_1 + Q(\eta)\frac{\partial^2}{\partial x^2}w_0].$$

Next, we integrate (17b) with respect to η, insert the above expression into this result, do an integration by parts to find

$$\kappa\frac{\partial}{\partial\eta}w_2 = \frac{\partial}{\partial t}w_0\int_0^\eta g(\eta')\,\mathrm{d}\eta' - \hat{\kappa}\eta\frac{\partial^2}{\partial x^2}w_0 - P|u_0|^2\int_0^\eta f(w_0,\eta')\,\mathrm{d}\eta' + \kappa(\frac{\partial}{\partial x}a_1 + Q(\eta)).$$

We again require that $\dfrac{\partial}{\partial\eta}w_2$ is bounded as $\eta\to\infty$. Since $\kappa(\dfrac{\partial}{\partial x}a_1 + Q(\eta))$ is bounded we deduce (19).

Acknowledgements

The work of B.S. Tilley was supported by a grant from the National Science Foundation (DMS-9971383). The work of G. A. Kriegsmann was supported by grants from the National Science Foundation (DMS-0071368) and the US Department of Energy (DE-FG02-94ER25196).

References

1. D. Jaglin and J. Binner, Densification of woven fiber SiC/SiC composites by microwave enhanced chemical vapor infiltration. In: D. Sanchez-Hernandez *et al.* (eds.), *7th International Conference on Microwave and High Frequency Heating* (1999) pp. 283–286.
2. A. Ditkowski, D. Gottleib, and B. W. Sheldon, On the mathematical analysis and optimization of chemical vapor infiltration in materials science, *Math. Mod. Num. Analysis* 40 (2000) 337–351.
3. T. L. Starr and A. W. Smith, 3-D modeling of forced-flow thermal-gradient CVI for ceramic composite fabrication. In: T. M. Besmann and B. M. Gallois (eds.), *Materials Research Special Symposium* 168 (1990) pp. 55–60.
4. S. V. Sotirchos, Dynamic modeling of chemical vapor infiltration, *AIChE J.* 37 (1991) 1365–1378.
5. D. Gupta and J. W. Evans, A mathematical model for chemical vapor infiltration with microwave heating and external cooling, *J. Materials Res.* 40 (1991) 810–818.
6. D. Gupta and J. W. Evans, Calculation of temperatures in microwave-heated two-dimensional ceramic bodies, *J. Amer. Ceramic Soc.* 76 (1993) 1915–1923.
7. D. Gupta and J. W. Evans, Mathematical model for chemical vapor infiltration in a microwave-heated preform, *J. Amer. Ceramic Soc.* 76 (1993) 1924–1929.

8. B. S. Tilley and G. A. Kriegsmann, Microwave-enhanced chemical vapor infiltration: a moving interface model. *Microwaves: Theory and Application in Materials Processing V (Ceramic Transactions)* 80 (2001) 3 –10.
9. B. S. Tilley and G. A. Kriegsmann, Microwave-enhanced chemical vapor infiltration: a sharp interface model. *J. Eng. Math.* 41 (2001) 33–54.
10. G. A. Kriegsmann, Electromagnetic wave propagation in periodic porous structures. *Wave Motion*, in press.
11. G. A. Kriegsmann, Thermal runaway in microwave heated ceramics: a one-dimensional model, *J. Appl. Phys.* 71 (1992) 1960–1966.
12. J. A. Pelesko and G. A. Kriegsmann, Microwave heating of ceramic laminates, *J. Eng. Math.* 32 (1997) 1–18.
13. J. Kevorkian and J. D. Cole, *Multiple Scale and Singular Perturbation.* Applied Mathematical Science Series, Volume 114. New York: Springer (1996) 632 pages.